

## Investigation in Gas-Oil Two-Phase Flow using a Differential Pressure Transducer and Wire Mesh Sensor in Vertical Pipes

Veyan A. Musa<sup>1</sup>, Raid A. Mahmood<sup>1,2</sup>, Sherwan M. Simo<sup>3</sup>,  
Abbas Kh. Ibrahim<sup>3</sup>, Lokman A. Abdulkareem<sup>3,4</sup>

<sup>1</sup>Department of Mechanical Engineering, University of Zakho, Zakho city, Kurdistan Region of Iraq, Iraq

<sup>2</sup>School of Mechanical and Electrical Engineering, University of Southern Queensland, Australia

<sup>3</sup>Department of Petroleum Engineering, University of Zakho, Zakho city, Kurdistan Region of Iraq, Iraq

<sup>4</sup>Institute of Fluid Dynamics, Helmholtz-Zentrum Dresden-Rossendorf, Dresden, Germany

Correspondence Author: veyan.musa@uoz.edu.krd

*Received September 10, 2022; Revised October 11, 2022; Accepted November 13, 2022*

### Abstract

The current study is performed to identify the flow regimes of oil-gas two-phase flow experimentally in a vertical pipe has an internal diameter of 6.7 cm. It also aims to provide more details about the possibility of using Differential Pressure Transducers (DPT) for indicating flow patterns. A flow development of oil and gas has been investigated in a vertical pipe of 6 m in length and operated at atmospheric pressure. A series of experiments have been run to cover a range of inlet oil superficial velocities from 0.262 to 0.419 m/s, and inlet gas superficial velocities from 0.05 to 4.7 m/s. Wire Mesh Sensors (WMS) have been used to collect the obtained void fraction values of the flow. The Differential Pressure Transducer (DPT) is utilized to measure the pressure drop values of a one-meter along the pipe. The flow patterns are classified according to the analysis of void fractions, pressure gradients regarding time series, tomographic images, probability density functions of the void fractions, and pressure gradients. A bubbly flow is observed at low superficial velocities of gas and liquid, slug flow is observed at the lower flow rate of liquid and moderate flow rates of gas, while the churn flow pattern is recognized at the higher rates of liquid and gas. Also, the result has revealed the possibility of using Differential Pressure Transducers (DPT) to classify the gas-oil flow patterns in vertical pipes.

**Keywords:** Wire-mesh sensor, Pressure drops in pipes, Two-phase flow pattern, Differential Pressure transducers (DPT).

## 1. INTRODUCTION

Two-phase flow including oil-gas is involved in various industrial and engineering sectors. The oil-gas two-phase flow can be found in pipeline networks and petroleum refinery processes [1], [2]. The flow of oil gas in pipes can reform its structure continuously depending on the thermodynamic properties and flow operation conditions like phases' velocities, pipe inlet diameter, and pressure [3]. Parameters like the operating velocities and pressure drops are considered very consequential for designing an efficient pumping system [4], [5].

Engineering designers need to set up efficient transportation pipe networks, and also reduce pipeline cross-section and cracking. Pressure drops that occurred in pipes of different orientations are affected by the flow structure. Pressure drops are considered a huge challenge for designers to select the required pump or the diameter of pipes. There are many techniques to reduce the pressure drop in pipelines such as inserting a guide vane. It can reduce pressure drop and flow separation [6]. The investigation of such nonhomogeneous flow still requires more information to forecast the flow development under the pressure drop through vertical pipes. Besides, the validation of utilizing DPT sensor, as a considerably cheap technique compared with WMS, to dedicate the developed flow patterns in pipes is essentially requirable. Also, this study provides more experimental information about gas-oil flow considering the pressure drop, and more databases for future experimental and computational research to classify the flow structure of two-phase.

## 2. RELATED WORKS

Liu et al. [7] studied the Friction pressure drop models in a mixture of gas-liquid in pipes at high liquid and gas velocities. They reported the impact of phases' velocities on the pressure drop, where the outcome indicates that the pressure drop rises with the increment of both velocities. Wallis [8] concluded a mathematical equation of the behavior of liquid hold-up and pressure drops. His argument assumed that pressure drops were associated with two-phase patterns, also he summarized that pressure drops of the two-phase flow component were higher than the estimated pressure drops of the single flow individually. Lin [9] predicted the flow pattern of the upward inclined pipes with orientations of 0 to 90° by utilizing deep-learning neural networks. The author developed a model that was validated with the outcomes of its experiment, also the result was compared with the flow regime map. Another study was carried out by Dang et al. [10], they studied the characteristics of air-water, where it has been constructed on bubbly-to-slug transition flow in a vertical tube of an internal diameter of 12.7 mm. The study was performed with liquid velocities ranging from 0.3 to 2.0 m/s, and void fractions varied from 0.07 to 0.66. The outcome indicated that the distribution of wall-peak void fractions disappeared in the smaller tube's

diameter when the flow was bubbly to slug, and the distribution was related to bubble size and void fractions.

Wire Mesh Sensors (WMSs) and Differential Pressure Transducers (DPTs) were used in the current paper to identify the void fractions and the differential pressure drops of two-phase flow are improved as reliable sensors through numerous published papers such as [11], [12], [13], [14], [15]. While the Wire Mesh Sensor (WMS) is based on the analysis of void fractions to observe the phase distribution with a high resolution, the Differential Pressure Transducers (DPT) recorded the simultaneous pressure drops of two-phase flow in a specified distance along a pipe. WMS was introduced firstly by Prasser et al. [11] as an intrusive tomographic image sensor that can be relied on to estimate cross-sectional void fractions of the flow. Pressure drops fluctuation of a two-phase flow in pipes is very nearly connected with the behavior of flow patterns. Chalgeri and Jeong [16] studied the vertical two-phase flow in a vertical rectangular channel using a DPT. The outcome showed the possibility of using the sensor for classifying the two-phase flow structures, where many flow patterns were classified such as bubbly flow.

The validation of using DPT is investigated by Musa et al. [17] in a pipe of an internal diameter of 50 mm with different directions; 0, 30, and 45 degrees, they denoted that the pressure in the tested pipe is dropping with the increasing of the void fraction's ratio, also the usage of DPT as a sensor for indicating flow patterns is acceptable with 30- and 45-degrees pipe orientations. The two-phase flow has been investigated experimentally by the authors in [18], [19]. The tests examined the flow pattern in a pipe of a diameter of 6.7 cm at various superficial velocities, they classified the flow patterns by analyzing; the Probability Density Function (PDF) and the time series of void fractions. Bubbly and churn flow patterns are observed in the vertical pipe at lower and higher flow rates of air. An empirical investigation was conducted by Abdulkadir et al. [20] to study the flow regime of air-silicone oil flow in a riser vertical pipe using the flowing sensors; Electrical Capacitance Tomography (ECT), WMS, and DPT for detection of the void fractions and pressure drop fluctuation. The Mean Square Error methods were utilized to analyze the result. Cap bubbles, slug, and churn flows are dedicated.

Adaze et al. [21] presented a computational fluid dynamic for two-phase flow. The authors reported that the CFD technique is flexible way but it is a bit complex to obtain convergence. Yang et al. [22] tested the two-phase flow in different pipe sizes, and they identified four various flow regimes; bubbly, cap bubbly, churn turbulent, and annular flow were observed using the method of artificial neural network. Qiao et al. [23] investigated the structural impacts of inlets on the parameters of two-phase flow in the vertical flow of air and water. Flow regime maps were moderated for the flow regimes.

### 3. ORIGINALITY

Although many studies and techniques presented the estimation of pressure drop for two-phase flow, there is insufficient information about the experimental estimation and real database for the pressure drop and flow pattern in the vertical pipe. Therefore, this study presents an experimental estimation and real database for the oil-gas two-phase flow in a vertical pipe.

### 4. EXPERIMENT AND SYSTEM DESIGN

The current experiment was performed at atmospheric pressure utilizing a mixture flow consisting of gas and oil. A typical mixer is joined to the test structure for combining the entered fluids. The oil is injected by a centrifugal pump at a constant inlet of liquid velocities ( $U_{sl}$ ) 0.262 and 0.419 m/s, while the air is produced by a central compressor at different velocities ( $U_{sg}$ ) altered from 0.05 to 4.9 m/s. The tested vertical pipe is made from acrylic with a diameter of 6.7 cm. The number of tested runs is 26 covering the various velocities of gas and liquid as mentioned above under the lab restriction. A set of measuring instruments is used to record the experimental data. Based on its manufacture datasheet, its accuracy has been considered as shown in Table 1.

**Table 1.** Specification of measuring instruments

Instrument	Range	Accuracy
Pump (Flowserve model 32WJ200)	Maximum flow capacity 4 m <sup>3</sup> /s	± 0.038
Rotameter (KDG, France)	0 -2.4 m <sup>3</sup> /s	± 0.03
Rotameter (Fisher 2000)	6-60 m <sup>3</sup> /s	± 0.035
Gage pressure (BUDENBERG)	0-103.4 KPa	± 0.044

Flow patterns are examined by a special type (Rosemount 2024 DP cell, range 0-750 in H<sub>2</sub>O, manufacture uncertainty=± 0.04) of Differential Pressure Transducer (DPT) which is used to record the total pressure gradients of 1-meter length, and a tomographic Wire Mesh Sensor (WMS) of (24×24) wires arrangement design is fixed cross-sectionally against the flow to record the void fractions at 1000 frame/s. For the downstream flow, a cyclone is exploited to separate the phases and inforced liquid to enter a large take. The test is arranged as Figure 1 depicted where a storage container is used to maintain the temperature of the oil at room temperature (27 °C).

The pipe pressure is associated with the local superficial velocity of the gas ( $U_{sg}$ ). Equations 7 and 8 are used to obtain the local  $U_{sg}$  from the inlet  $U_{sg}$  as illustrated in [24]. The local  $U_{sg}$  values were influenced by the pressure drops that reformed along the vertical pipe where their values showed a little difference. The calculated local  $U_{sg}$  values of the 26 tests are stated in Tables 2 and 3.

Data acquisition is utilized to collect the electrical signals ( $\Delta P_{read}$ ) that arrived from the DPT sensor, and then those data are used to analyze the results as stated in Equations 1, 2, 3, 4, and 5.

$$\Delta P_{read} = (P_1 + \rho_{liq} g Z_1) - (P_2 + \rho_{TP} g Z - \rho_{liq} g Z_2) \quad (1)$$

$$\left(\frac{dp}{dz}\right)_{fric} = \frac{\rho_{liq} g Z - \Delta P_{read} - \rho_{TP} g Z}{Z} = \frac{p_2 - p_1}{Z}, \quad (2)$$

$$\left(\frac{dp}{dz}\right)_{Total} = \frac{(p_2 + \rho_{TP} g H) - p_1}{Z} = \frac{\rho_1 g H - \Delta P_{read}}{Z} = \left(\frac{dp}{dz}\right)_{fric} + \rho_{TP} g, \quad (3)$$

$$\rho_{TP} = \alpha_{gas} \rho_{gas} + (1 - \alpha_{gas}) \rho_{liq}, \quad (4)$$

$$\left(\frac{dp}{dz}\right)_{Total} = \left(\frac{dp}{dz}\right)_{fric} + \left(\frac{dp}{dz}\right)_{acce} + \Delta z g (\alpha \rho_{gas} + (1 - \alpha) \rho_{liq}). \quad (5)$$

Where  $\rho_{liq}$ ,  $\rho_{gas}$  and  $\rho_{TP}$  are liquid density, gas density, and total density at recorded pressure respectively.  $Z$  is the potential heat and  $g$  is the gravitational acceleration.  $H$  is static heat and  $P$  is pressure.  $\left(\frac{dp}{dz}\right)_{Total}$ ,  $\left(\frac{dp}{dz}\right)_{fric}$ ,  $\left(\frac{dp}{dz}\right)_{acce}$  are the total, frictional, and acceleration pressure drops in Pa.  $\alpha_{gas}$  is the void fraction of the gas phase.

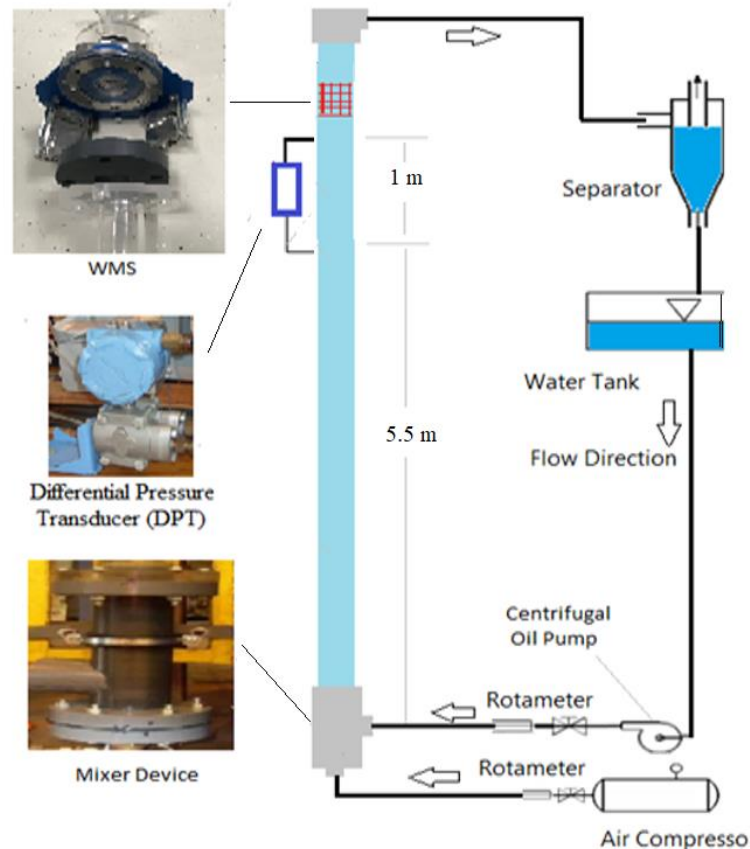


**Figure 1.** Experiment Layup.

The pressure drops produced by the flow acceleration are omitted because the distance between the two legs of the DPT was one meter and it's considered small. The fractional pressure drops have remained stable along with this distance. A special program related to the WMS sensor (CapWMS\_display) is used to simulate the cross-sectional flow and represent it by tomographic images.

Sensors are calibrated and tested properly to obtain precise readings in the vertically tested pipe. The WMS is situated crossing the flow rate, and it is associated with an electronic circuit and connected to a computer. The volume of the tested vertical pipe is determined.  $V_{max}$  and  $V_{min}$  represented the maximum and minimum dimensionless voltage values that were recorded when the pipe is filled with oil and gas consequently. The final voltage  $V$  in Equation 6 is estimated from the reading voltage  $V_{read}$  and corresponds with void fraction ( $\alpha$ ) values.

$$V = \frac{V_{read} - V_{min}}{V_{max} - V_{min}} \quad (6)$$

The DPT has also been calibrated utilizing the relationship between the differential pressure of a one-meter pipe length and the output voltage using special lab software, A/D board NI-6034E (National Instruments), and data acquisition. The data acquisition joined with a personal computer where converted the physical values depending on the results to an output voltage. More information about WMS and DPT can be found in [24]. Liquid rotameter has been calibrated also regarding the operating conditions such as temperature and viscosity. Thus, a liquid pump is turned on for collecting an amount of oil volume at a specific time. By measuring the collected volume, the rotameter reading is fixed.

The pipe pressure is associated with the local superficial velocity of the gas ( $U_{sg}$ ). Equations 7 and 8 are used to obtain the local  $U_{sg}$  from the inlet  $U_{sg}$  as illustrated in [24]. The local  $U_{sg}$  values were influenced by the pressure drops that reformed along the vertical pipe where their values showed a little difference. The calculated local  $U_{sg}$  values of the 26 tests are stated in Tables 1 and 2.

$$U_{sg} = m / [\rho_p A_p] \quad (7)$$

$$m = \rho_A Q \sqrt{\rho_R} \quad (8)$$

Where,  $\rho_p = 1.2$  Pp = the gas density at pipe pressure,  $\rho_R =$  the gas density at reference equal to 1.2,  $\rho_A = 1.2$  PA where its reference to the gas density at various area meters, and PA is the pressure at that area.

**Table 2.** Local Usg corrected with pressure drop values in the vertical pipe at Usl=0.262 m/s

Run	Inlet Usg (m/s)	Pressure drop (kPa/m)	Local Usg (m/s)
1	0.050	6301	0.060
2	0.062	6164.1	0.078
3	0.280	5068.2	0.353
4	0.340	4862.7	0.419
5	0.400	4725.8	0.490
6	0.500	4383.3	0.651
7	0.700	4109.4	0.841
8	0.900	3835.4	1.111
9	1.400	3698.4	1.658
10	1.900	3424.5	2.189
11	2.360	3492.9	2.743
12	2.830	3629.9	3.308
13	4.700	4794.3	5.743

**Table 3.** Local Usg corrected with pressure drop values in the vertical pipe at Usl=0.419 m/s

Run	Inlet Usg (m/s)	Pressure drop (kPa/m)	Local Usg (m/s)
14	0.05	6506.5	0.0607
15	0.06	6301	0.0784
16	0.28	5342.2	0.3568
17	0.34	4931.2	0.4201
18	0.40	4931.2	0.4938
19	0.50	4657.3	0.6575
20	0.70	4383.3	0.8495
21	0.90	4109.4	1.1219
22	1.40	3972.4	1.6747
23	1.90	3903.9	2.2275
24	2.36	4109.4	2.8048
25	2.83	4314.8	3.3901
26	4.70	5753.1	5.9259

During the test, some unreasonable data are executed because of system failure from the WMS software and the electrical parts. The uncertainty has been considered in this study [25] and used by many researchers such as Hameed et al [26], and Mahmood et al. [27]. The maximum experimental uncertainty for the gas velocity is recorded at  $\pm 0.037$  m/s based on the manufacturer uncertainty of the DPT which is equal to  $\pm 0.04\%$ .

## 5. RESULT, ANALYSIS, AND DISCUSSION

The developed flow patterns of two-phase flow in the tested pipe are classified using the following correlations and methods: Probability Density Function (PDF) plots of void fractions, void fractions with time series, tomographic images, PDF plots of pressure gradients, and pressure gradients

with time series. Flow void fractions are collected by utilizing the Wire Mesh Sensor (WMS) while the values of pressure gradient are obtained by the Differential Pressure Transducer (PDT). The mentioned correlations above are used successfully to estimate the flow patterns by the researchers in [1], [10], [13], [15], and [28]. A comparison is performed between the result estimated by the WMS and PDT to assess the validation of using the PDT for identification flow patterns.

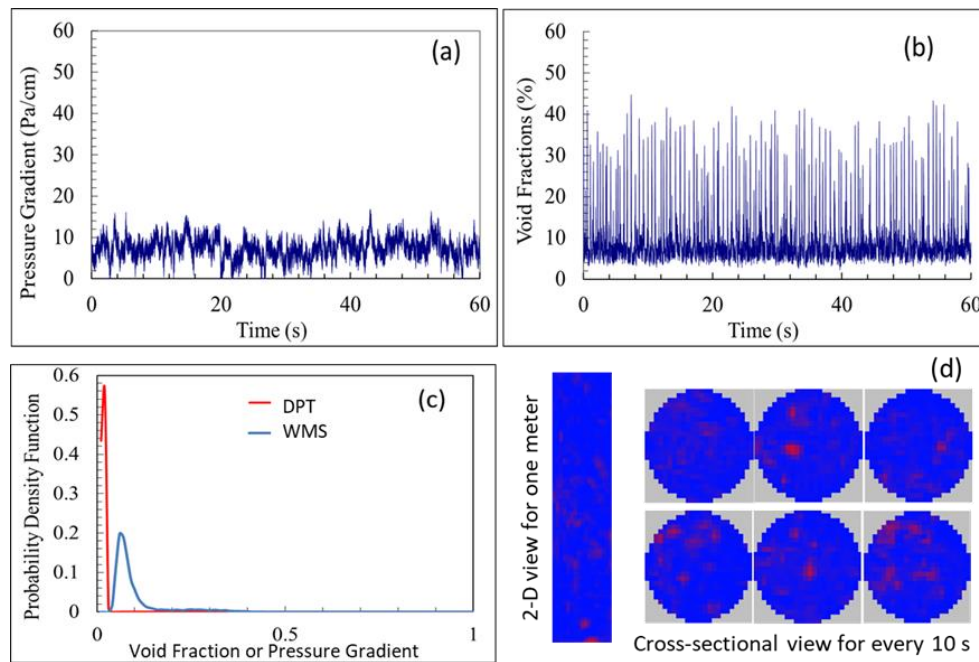


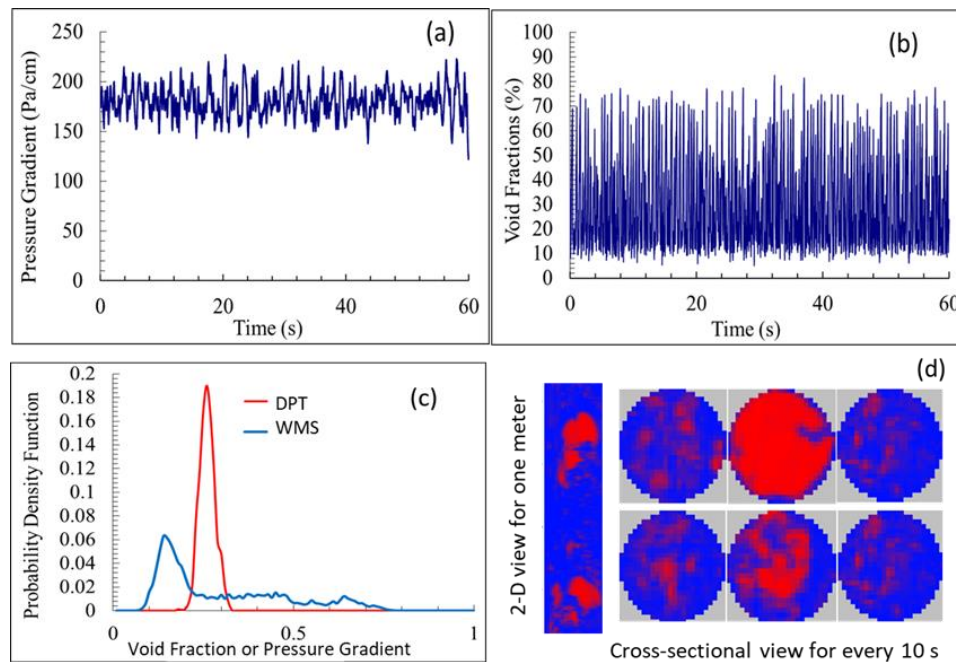
**Figure 2.** (a) pressure gradients with time series, (b) void fractions with time series, (c) PDFs of void fractions and pressure gradients, and (d) tomographic images, for bubbly flow at  $U_{sl} = 0.262$  m/s and  $U_{sg} = 0.05$  m/s

Bubbly flow is observed at the values of liquid velocity ( $U_{sl}$ ) 0.263 m/s and gas velocities ( $U_{sg}$ ) 0.051 m/s. The bubbles feature is observed from the tomographic images as shown in Figure 2d, where the gas is represented by red color and the oil in blue. The images are captured in 2-D view for one meter along the pipe length, and 2-D cross-sectionally views every 10 seconds. The bubbly flow pattern is observed as a laminar flow at a high amount of oil is interrupted with tiny gas bubbles distributed randomly along the pipe. The average frequencies of pressure gradient and void fractions are noticed at nearly 10 with the time series as illustrated in Figure 2. The PDF's plot of void fractions using WMS recorded 0.2 at a low void fraction value of 0.1. Similarly, The PDF's plot of pressure drops using DPT reached 0.6 at a low-pressure gradient value of 0.05 (Figure 2c).

As Figure 3a demonstrated, slug flow is categorized when the  $U_{sg}$  value is raised to 0.28 m/s at the fixed  $U_{sl}$  value of 0.262 m/s. The additional amount of gas produced slugs that lead up to an increase in the pressure drop, as a result of that, the frequency of pressure gradients with time

increased from 10 to 200 Pa/cm. In the same direction, the fluctuation range of void fractions is ranged between 10 and 70% (Figure 3b). The PDF plots of void fractions and pressure gradients showed two peaks at 0.06 and 0.18 respectively (Figure 3c). The cross-sectional tomographic image depicted bubbles coalesced to form slugs due to the increase in gas flow rate (Figure 3d). The analysis of void fractions utilizing WMS and pressure gradients Using DPT presented a reasonable confirmation regarding the behavior of their fluctuations, similar to the PDFs curves.

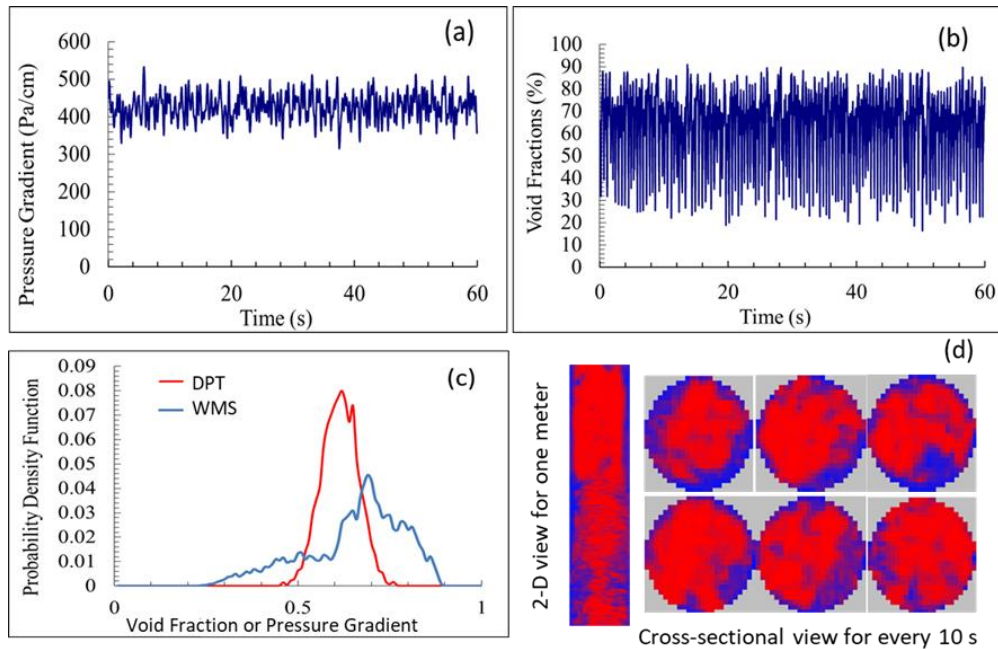
Two peaks are indicated for both PDF plots of void fractions and pressure gradients at 0.04 and 0.8 as Figure 4c displays. The peaks' location are recorded at considerably higher values of void fraction and pressure gradients. The frequency of the time series is denoted at higher pressure drop values near 450 Pa/cm (Figure 4a), while the fluctuation of void fractions was around 70% as noticed in the same figure (Figure 4b). The characteristic of the PDF plots, also the analysis of time series are referred to as churn flow patterns at  $U_{sl}$  value of 1.4 m/s. The increment of the gas amount was changing the flow pattern from slug to churn. As shown in Figure 4d, the tomographic images are confirmed by the above analysis.



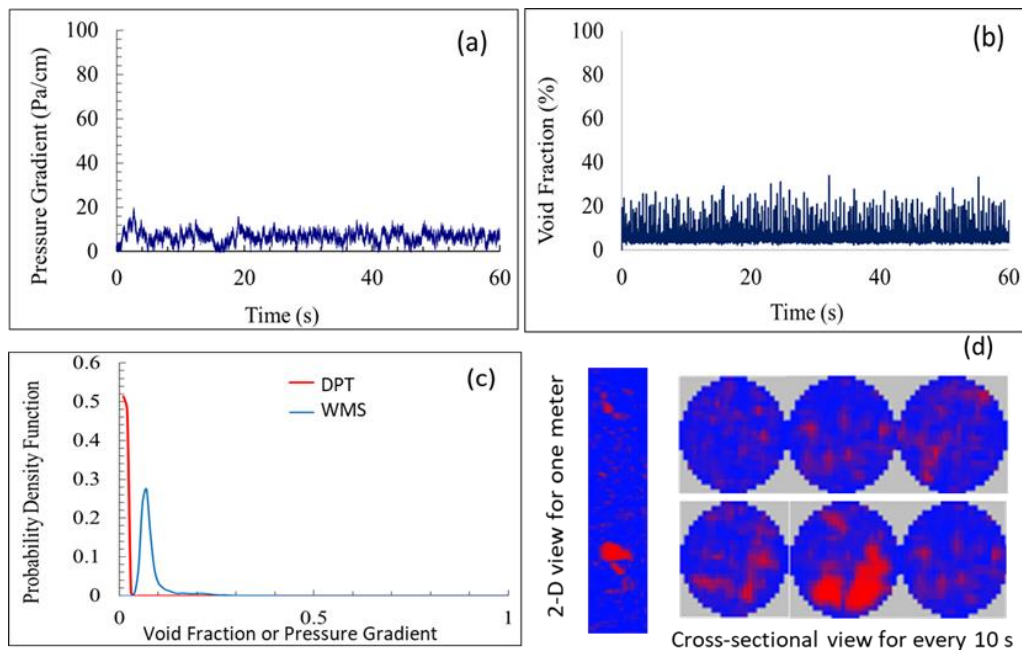
**Figure 3.** (a) pressure gradients with time series, (b) void fractions with time series, (c) PDFs of void fractions and pressure gradients, and (d) tomographic images, for slug flow at  $U_{sl} = 0.262$  m/s and  $U_{sg} = 0.28$  m/s

Also, the flow patterns are tested at the fixed value of  $U_{sl}$  0.419 m/s, where the bubbly flow is estimated at  $U_{sg}$  value ranging from 0.05 to 0.28 m/s with the increasing amount of oil as depicted in Figure 5. Slug flow is observed when the value of  $U_{sg}$  is altered from 0.34 to 1.9 m/s as illustrated in Figure 6. In addition, churn flow is identified at higher superficial velocities

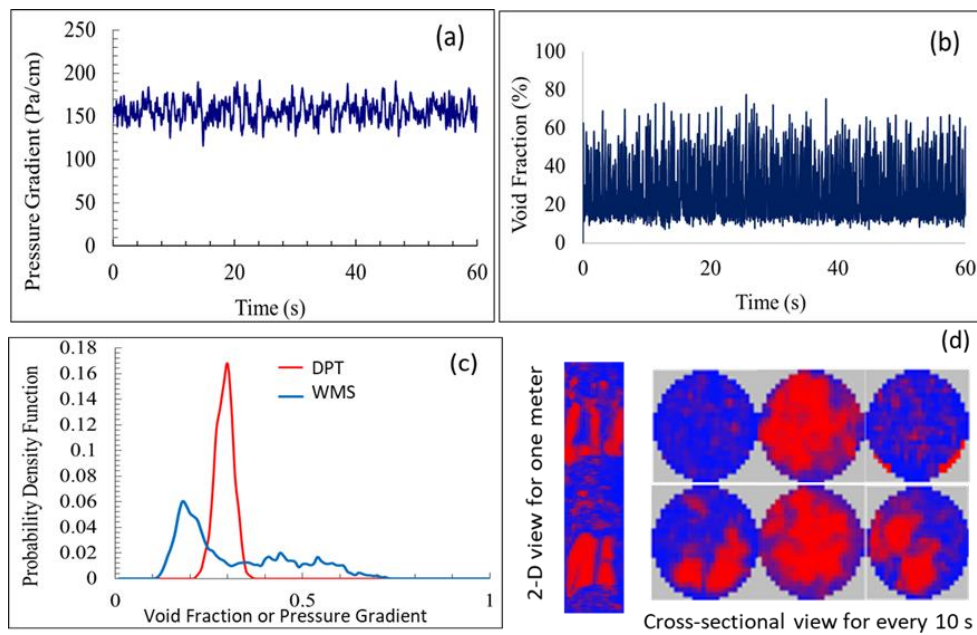
of the gas are varied from 2.36 to 4.7 m/s as demonstrated in Figure 7. The flow patterns are classified regarding the characteristics of the tomographic images, the analysis of PDF plots of pressure gradients and void fractions, and the analysis of time series.



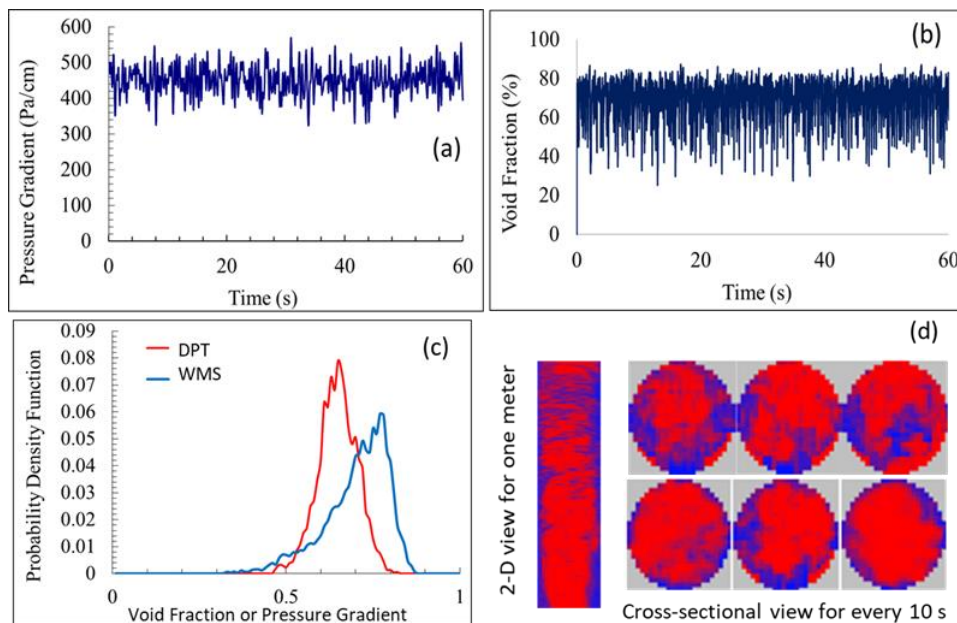
**Figure 4.** (a) pressure gradients with time series, (b) void fractions with time series, (c) PDFs of void fractions and pressure gradients, and (d) tomographic images, for churn flow at  $U_{sl} = 0.262$  m/s and  $U_{sg} = 1.4$  m/s



**Figure 5.** (a) pressure gradients with time series, (b) void fractions with time series, (c) PDFs of void fractions and pressure gradients, and (d) tomographic images, for bubbly flow at  $U_{sl} = 0.419$  m/s and  $U_{sg} = 0.05$  m/s



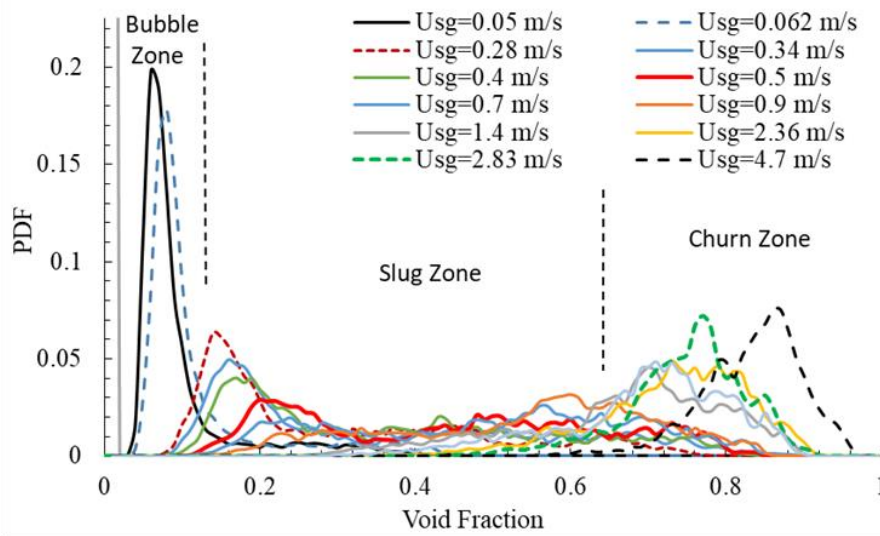
**Figure 6.** (a) pressure gradients with time series, (b) void fractions with rime series, (c) PDFs of void fractions and pressure gradients, and (d) tomographic images, for slug flow at  $U_{sl} = 0.419$  m/s and  $U_{sg}=0.34$  m/s



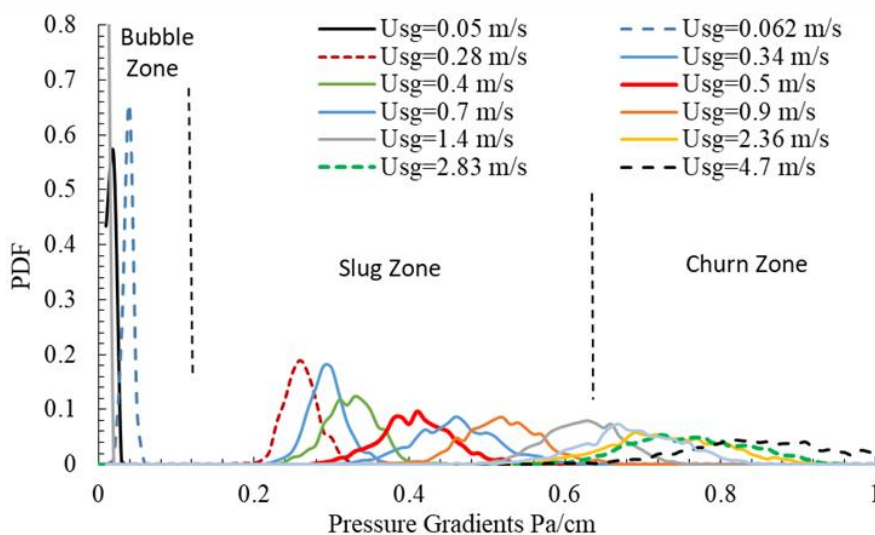
**Figure 7.** (a) pressure gradients with time series, (b) void fractions with rime series, (c) PDFs of void fractions and pressure gradients, and (d) tomographic images, for churn flow at  $U_{sl} = 0.419$  m/s and  $U_{sg}=1.9$  m/s

Figure 8a showed the plots of void fractions PDF obtained for different values of  $U_{sg}$  ranging from 0.05 to 4.7 m/s at the fixed  $U_{sl}$  value of 0.262 m/s, where those plots are compared with the pressure gradients plots of PDF in Pa/cm at the same operating condition (Figure 8b). Generally, both plots

conducted the same behavior. For the bubbly flow patterns zone, both plots had higher values of PDF at lower void fractions and pressure gradients. For the slug flow patterns zone, similar behavior is observed for the plots, it showed fluctuation values PDF of void fractions ranged between 0.2 to 0.4 at void fractions values scoped from 0.1 to 0.65, also the fluctuation of PDF of pressure gradients are noticed between 0.1 to 0.2 at pressure gradients values ranging from 0.2 to 0.65. For the churn flow patterns zone, it is indicated the moderated values of PDF with void fractions compared to the lower values of PFD with Pressure gradients. Similarly, Figure 9 is introduced almost the same approach with a little alteration in zone position due to the increased value in  $U_{sl}$  to 0.419 m/s.

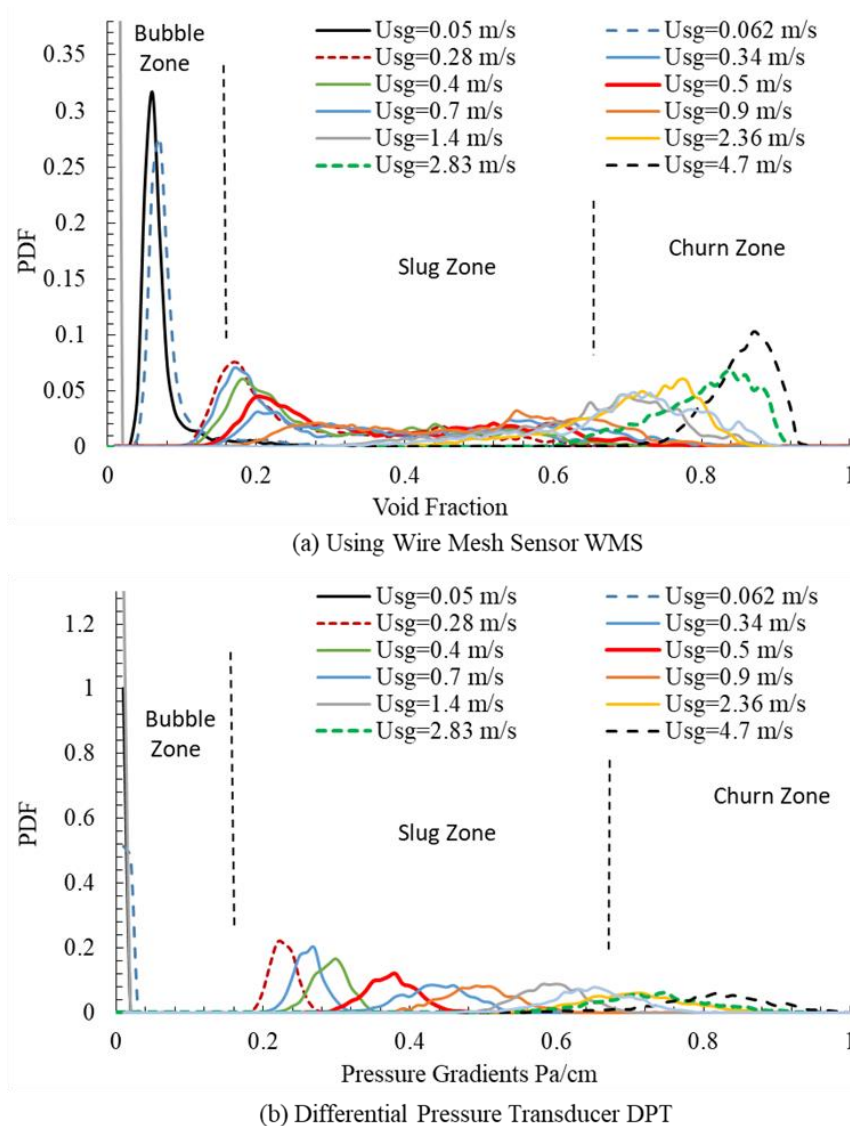


(a) Using Wire Mesh Sensor WMS



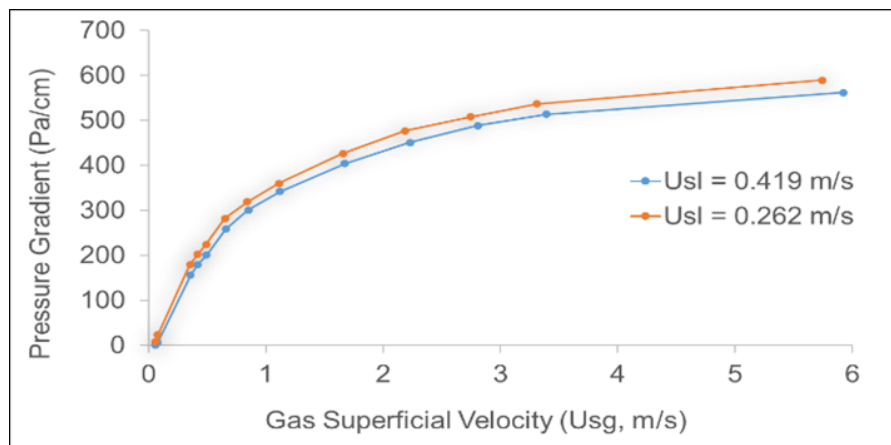
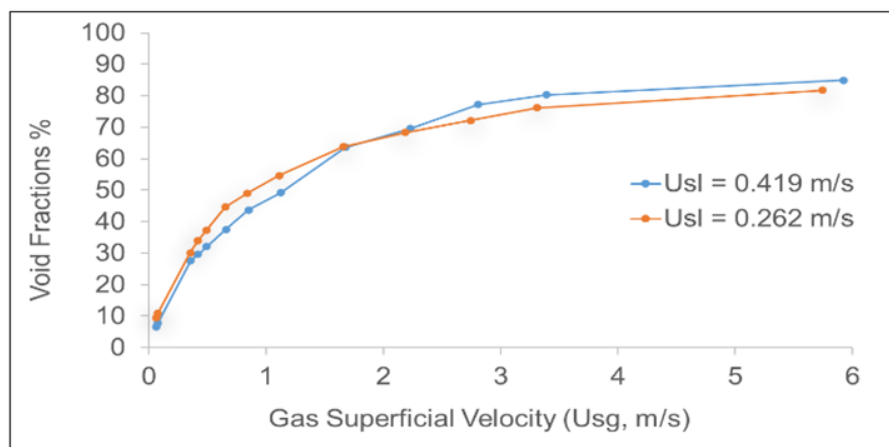
(b) Differential Pressure Transducer DPT

**Figure 8.** The PDF plots of void fraction and pressure gradients at  $U_{sg}$  varied from 0.051 to 4.7 m/s and  $U_{sl} = 0.2621$  m/s



**Figure 9.** The PDF plots of void fraction and pressure gradients at  $U_{sg}$  varied from 0.051 to 4.7 m/s and  $U_{sl} = 0.4191$  m/s

A comparison is carried out between the two arranged charts of the tested data for the current study. The charts are based on the relationship between the average pressure drops and gas superficial velocities as Figure 10a shows, and between the average void fractions and gas superficial velocities at the fixed values of superficial liquid velocity 0.262 and 0.419 m/s in a vertical pipe as depicted in Figure 10b. The plot's tendency presented the same behavior for both charts. Pressure gradients increased sharply with  $U_{sg}$  at lower values of gas flow rate, where this increment slowed down at moderate and higher values of  $U_{sg}$  rates, also the same behavior is observed for void fractions, which were obtained by WMS.

a) Pressure gradients (Pa/cm) with different  $U_{sg}$  rates (m/s)b) Void Fractions (%) with different  $U_{sg}$  rates (m/s)

**Figure 10.** The PDF plots of void fraction and pressure gradients at  $U_{sg}$  varied from 0.051 to 4.7 m/s and  $U_{sl} = 0.2621$  m/s

## 6. CONCLUSION

The present test is carried out using a mixture of gas and oil, two-phase flow in vertical pipes. The internal diameter of the tested pipe is 6.7 cm at atmospheric pressure and fixed flow temperature (27 C) to categorize the pressure drops and flow patterns in the pipe and also, to clarify the benefit of using the Differential Pressure Transducer (DPT) as validating cheap instrument compared with the Wire Mech Sensor (WMS) for identifying flow patterns. The study is concentrated on analyzing the pressure gradients and void fractions with time series in the range of accelerating the gas superficial velocity steeply from 0.051 to 4.9 m/s at constant values of oil superficial velocities 0.262 and 0.419 m/s.

Pressure gradients are increased with the increasing amount of gas flow rate due to the compressibility property of gas, thus the possibility of using DPT is reasonable because this is the same technique that is used in WMS where the fluctuation of void fractions values is used to sort flow

patterns. In the same direction, the fluctuations of pressure drops with time series are displayed the same characteristics contracted with the conduction of the void fractions with the time series, thus DPT can be utilized to estimate the flow patterns.

Bubbly, slug and churn flow patterns are specified at a fixed  $U_{sl}$  value of 0.2621 m/s and changed values of  $U_{sg}$  from 0.0603 to 0.0780 m/s, 0.3536 to 2.1890 m/s, and 2.7432 to 5.7436 m/s respectively, while the flow patterns at a fixed value of  $U_{sl}$  0.419 m/s are observed as a bubbly, slug and churn flow for  $U_{sg}$  value from 0.0607 to 0.3568 m/s, 0.0784 to 1.6747, and from 2.2275 to 5.9259 m/s respectively.

### Acknowledgments

The authors appreciate the College of Engineering Research Centre located at University of Zakho for the support that was provided to complete this work under grant number 9962.

### REFERENCES

- [1] Omar R., Hewakandamby B., Azzi A., and Azzopardi B. **Fluid Structure Behaviour in Gas-oil Two-phase Flow in a Moderately Large Diameter Vertical Pipe.** *Chemical Engineering Science*, 2018; 187: 377–390.
- [2] Ahmed S. K. B., Aliyu M. A., Baba Y. D., Abdulkadir M. Abdulhadi R. O., Lao L. and Yeung H. **Comparative Analysis of Riser Base and Flowline Gas Injection on Vertical Gas-Liquid Two-Phase Flow.** *Energies*, 2022; 15(19).
- [3] Zahedi R. and Babae Rad A. **Numerical and Experimental Simulation of Gas-liquid Two-phase Flow in 90-degree Elbow.** *Alexandria Engineering Journal*, 2021; 61(3): 2536-2550.
- [4] Zou S., Guo L., and Yao T. **Upstream-Flow-Based Mechanisms for Global Flow Regime Transition of Gas/Liquid Two-Phase Flow in Pipeline-Riser Systems.** *Chemical Engineering Science*, 2021; 240: 116542.
- [5] Mahmood RA, Saleh K, Musa VA, Massoud E, Sharifian-Barforoush A, Abdulkareem LA. **Two-Phase Flow Development of R134a in a Horizontal Pipe: Computational Investigation.** *International Journal of Heat and Technology*. 2021; 39(5): 1532–40.
- [6] Nugroho, S. and Hidayatulloh A.A., **Performance Analysis of The Effect on Insertion Guide Vanes For Rectangular Elbow 900 Cross Section.** *EMITTER International Journal of Engineering Technology*, 2016; 4(2): 358-370.
- [7] Liu Z. Liao R., Luo W., Ribeiro J. X. F., and Su Y. **Friction Pressure Drop Model of Gas-Liquid Two-Phase Flow in an Inclined Pipe with High Gas and Liquid Velocities.** *AIP Advances*, 2019; 9(8).
- [8] Wallis G. B. **One Dimensional Two Phase Flow.** USA: McGraw-Hill Book Company; 1969.

- [9] Lin Z, Liu X, Lao L, Liu H. **Prediction of Two-Phase Flow Patterns in Upward Inclined Pipes Via Deep Learning.** *Energy*. 2020;210: 118541.
- [10] Dang Z., Wang G., and Ishii M. **Two-phase interfacial structure of bubbly-to-slug transition flows in a 12.7 mm ID vertical tube.** *International Journal of Heat and Mass Transfer*, 2021; 165: 120556.
- [11] Prasser HM, Böttger A, Zschau J. **A new Electrode-Mesh Tomograph for Gas-Liquid Flows.** *Flow Measurement and Instrumentation*. 1998; 9(2): 111–9.
- [12] Wiedemann P., Döß A., Schleicher E., and Hampel U. **Fuzzy flow pattern identification in horizontal air-water two-phase flow based on wire-mesh sensor data.** *International Journal of Multiphase Flow*, 2019; 117: 153–162.
- [13] Vieira RE, Parsi M, McLaury BS, Shirazi SA, Torres CF, Schleicher E, et al. **Experimental characterization of vertical downward two-phase annular flows using Wire-Mesh Sensor.** *Chemical Engineering Science [Internet]*. 2015; 134:324–39.
- [14] Hernandez-Alvarado F., Kleinbart S., Kalaga D. V., Banerjee S., Joshi J. B., and Kawaji M. **Comparison of void fraction measurements using different techniques in two-phase flow bubble column reactors.** *International Journal of Multiphase Flow*, 2018; 102: 119–129.
- [15] Velasco Peña HF, Rodriguez OMH. **Applications of wire-mesh sensors in multiphase flows.** *Flow Measurement and Instrumentation*, 2015; 45: 255–73.
- [16] Chalgeri V. S. and Jeong J. H. **Flow regime identification and classification based on void fraction and differential pressure of vertical two-phase flow in rectangular channel.** *International Journal of Heat and Mass Transfer*, 2019; 132: 802–816.
- [17] Musa VA, Mahmood RA, Khalifa SMN, Ali OM, Abdulkareem LA. **Flow Patterns of Oil-Gas and Pressure Gradients in Near-Horizontal Flow Pipeline: Experimental Investigation Using Differential Pressure Transducers.** 2021; 39(2): 621–8.
- [18] Musa VA, Abdulkareem LA, Ali OM. **Experimental Study of the Two-Phase Flow Patterns of Air-Water Mixture at Vertical Bend Inlet and Outlet.** *Engineering, Technology & Applied Science Research*. 2019; 9(5): 4649–53.
- [19] Abdulkareem LA, Musa VA, Mahmood RA, Hasso EA. **Experimental Investigation of Two-Phase Flow Patterns in a Vertical to Horizontal Bend Pipe Using Wire-Mesh Sensor.** *Revista de Chimie*. 2021; 71(12): 18–33.
- [20] Abdulkadir M, Jatto DG, Abdulkareem LA, Zhao D. **Pressure drop, void fraction and flow pattern of vertical air-silicone oil flows using differential pressure transducer and advanced instrumentation.** *Chemical Engineering Research and Design*, 2020; 159(2012): 262–77.

- [21] Adaze E., Badr H. M., and Al-Sarkhi A. **CFD modeling of two-phase annular flow toward the onset of liquid film reversal in a vertical pipe.** *Journal of Petroleum Science and Engineering*, 2019; 175: 755–774.
- [22] Yang Z., Dang Z., Yang X., Ishii M., and Shan J. **Downward two phase flow experiment and general flow regime transition criteria for various pipe sizes.** *International Journal of Heat and Mass Transfer*, 2018; 125: 179–189.
- [23] Qiao S., Mena D., and Kim S. **Inlet effects on vertical-downward air-water two-phase flow.** *Nuclear Engineering and Design*, 2017; 312: 375–388.
- [24] Abdulkareem LA. **Tomographic investigation of gas-oil flow in inclined risers.** *PhD thesis, University of Nottingham*; 2011.
- [25] Coleman, H. W., and Glenn S. W. **Experimentation, validation, and uncertainty analysis for engineers.** *John Wiley & Sons*, 2018.
- [26] Hameed, A.I., L.A. Abdulkareem, and R.A. Mahmood, **Experimental Comparison Between Wire Mesh and Electrical Capacitance Tomography Sensors to Predict a Two-Phase Flow Behaviour and Patterns in Inclined Pipe.** 2021.
- [27] Mahmood R. A., Saleh K., Musa V. A., Massoud E., and Al-lwayzy S. H. **CFD Simulations and Experimental Observation for Air-Water Two-phase Flow in a Vertical Pipe.** *Gongcheng Kexue yu Jishu*. 2022; 54(06): 2363–2375.
- [28] Azzi A., Bouyahiaoui H., Berrouk A. S., Hunt A., and Lowndes I. S. **Investigation of fluidized bed behaviour using electrical capacitance tomography.** *Canadian Journal of Chemical Engineering*, 2020; 98(8): 1835–1848.